Lithium-Ion Batteries Hot Paper

DOI: 10.1002/ange.201405139

Organic Dicarboxylate Negative Electrode Materials with Remarkably Small Strain for High-Voltage Bipolar Batteries**

Nobuhiro Ogihara, Tomomi Yasuda, Yoshihiro Kishida, Tetsu Ohsuna, Kaito Miyamoto, and Nobuko Ohba*

Abstract: *As advanced negative electrodes for powerful and useful high-voltage bipolar batteries, an intercalated metal–organic framework (iMOF), 2,6-naphthalene dicarboxylate dilithium, is described which has an organic-inorganic layered structure of π-stacked naphthalene and tetrahedral LiO_4 units. The material shows a reversible two-electron-transfer Li intercalation at a flat potential of 0.8 V with a small polarization. Detailed crystal structure analysis during Li intercalation shows the layered framework to be maintained and its volume change is only 0.33 %. The material possesses two-dimensional pathways for efficient electron and Li^+ transport formed by Li-doped naphthalene packing and tetrahedral LiO_3C network. A cell with a high potential operating $LiNi_{0.5}Mn_{1.5}O_4$ spinel positive and the proposed negative electrodes exhibited favorable cycle performance (96 % capacity retention after 100 cycles), high specific energy (300 Wh kg^{-1}), and high specific power (5 kW kg^{-1}). An 8 V bipolar cell was also constructed by connecting only two cells in series.*

Research and development into rechargeable Li-ion batteries is of particular importance because of their potential as large-scale energy storage devices in automotive applications and stationary power-storage systems.[1] In such applications the cells are connected in series rather than used as a single cell to obtain high voltages. A high-voltage design would hence be desirable for large-scale applications. Compared to conventional Li-ion batteries that are connect in series (Figure 1 a), bipolar Li-ion batteries (Figure 1 b) provide several beneficial features such as 2) high voltage per unit cell, 2) low internal resistance through reduced terminal connections when a cell pack is assembled that connects the unit cells, and 3) high total volumetric energy density. The fabrication of bipolar cells requires a combination of bipolar electrodes and solid-state electrolytes, such as inorganic solid, polymer, and gel-polymer (gelled liquid) electrolytes, which are used to prevent short circuits in single bipolar electrodes. When compared with Al foil electroplated with a thin layer of Cu on one side, a bipolar electrode using only Al provides a clear advantage in terms of fabrication. Al and Cu are typically used as current collectors for positive and negative electrodes, respectively.

In bipolar batteries, the electrode potential is important for a high-voltage design because voltage is determined by the potential difference between the positive and negative electrodes. As shown in Figure 1 c, two basic types of intercalated electrode materials have been studied on a large scale for Li-ion batteries: lithium transition metal oxides[2] and graphitic carbon compounds,[3] which demonstrate durability because of the small changes in the volume (5–10 %) of their main structure during cycling. When designing a bipolar cell based on Al current collectors, graphitic carbon compounds operating at 0.1 V (versus Li/Li^+) cannot be used because Al reacts with Li at 0.4 V prior to the intercalation of Li into the graphitic carbon structures. Moreover, when lithium titanate ($Li_4Ti_5O_{12}$)[4] operating at 1.55 V is used, the cell voltage becomes very low and the total energy density decreases drastically. Therefore, an operating potential range of 0.5–1.0 V is essential for negative electrodes in high-voltage bipolar batteries. In addition, small changes in the volume (< 10 %) during cycling is indispensable for good performance. For example, layered $LiMS_2$ (M = Ti, V) with Ti^{3+}/Ti^{2+} and V^{3+}/V^{2+} redox couples have also been reported that demonstrate flat plateaus at approximately 0.5 and 1.0 V, respectively.[5] However, the capacities of these materials decrease on cycling because of a 30 % change in the volume during Li intercalation.[5b] Another research group has reported the redox properties of organic-based π-conjugated dicarboxylate dilithium salts[6] operating from 0.8 to 1.4 V. Similar materials have also been reported, such as π-conjugated dicarboxylate disodium salts[7] and π-conjugated dicarboxylate with dihydroxytetralithium salts.[8] However, these studies focused primarily on the molecular structure and have not discussed in detail the change in volume, the solid stage with intercalated Li^+ ions, or electron transport during Li intercalation. Such mechanisms significantly affect the cycle performance or rate capability; therefore, they are important for a full understanding of the detailed mechanisms.

We have focused on the nanostructures of the organic-based π-conjugated dicarboxylate salts formed by molecular self-assembly and propose an electroactive material based on π-conjugated dicarboxylate with an intercalated metal–organic framework (iMOF) that operates at the target potential (Figure 1 c).[9] MOFs are crystalline materials com-

[*] Dr. N. Ogihara
Toyota Central R&D Laboratories Inc.
Nagakute, Aichi, 480-1192 (Japan)
E-mail: ogihara@mosk.tytlabs.co.jp
T. Yasuda, Y. Kishida, Dr. T. Ohsuna, K. Miyamoto, Dr. N. Ohba
Toyota Central R&D Laboratories Inc. (Japan)

[**] We acknowledge Prof. H. Uekusa of the Tokyo Institute of Technology for powder XRD analysis of the pristine sample, Dr. R. Asahi for guidance with the first-principles calculations, T. Okuda for preparation of the bipolar cell, and Dr. M. Shiozawa for SEM observations.

Supporting information for this article is available on the WWW under http://dx.doi.org/10.1002/anie.201405139.

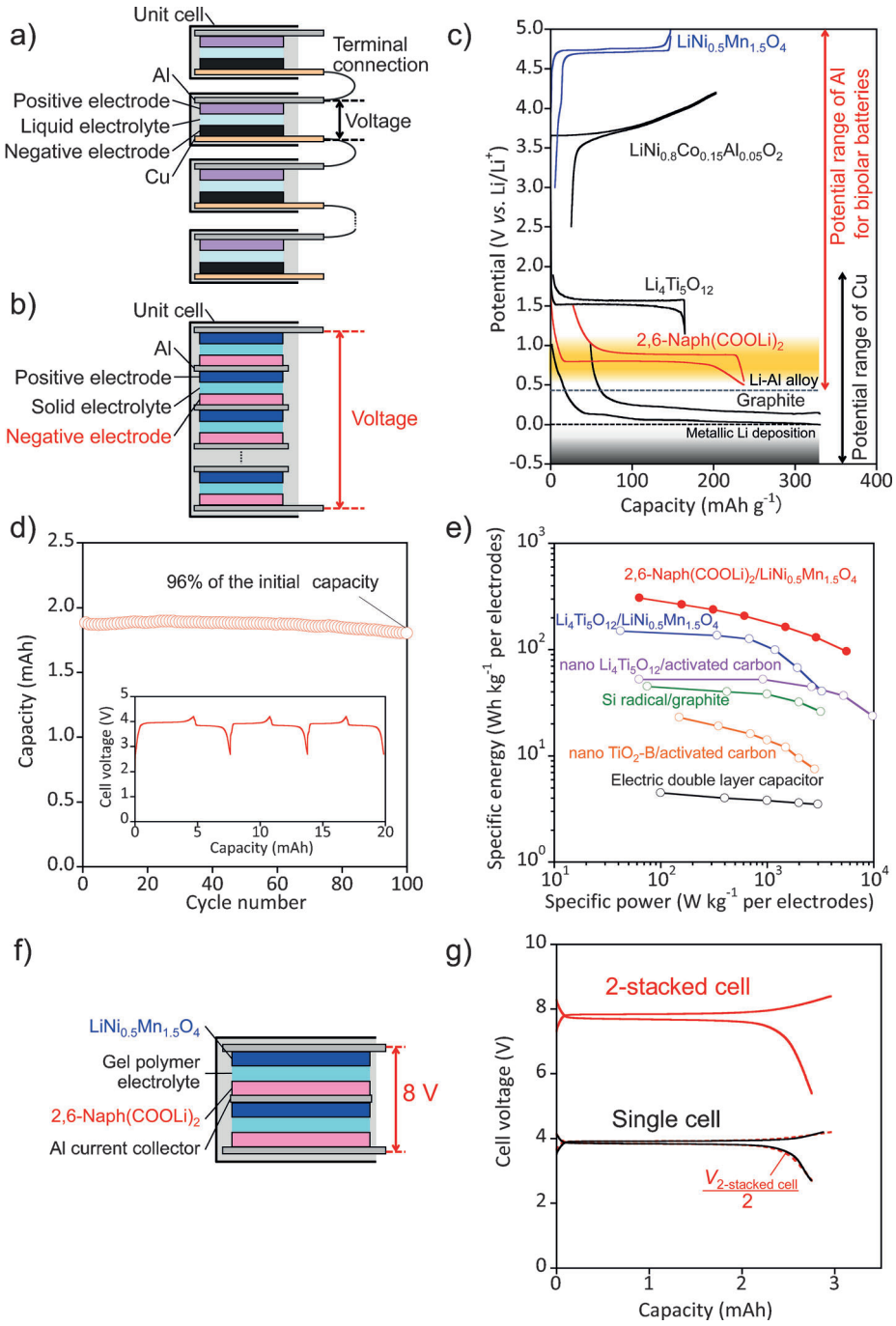

Figure 1. The concept towards future high-voltage bipolar batteries. a) Li-ion batteries connected in series. b) Proposed high-voltage bipolar Li-ion batteries. c) Comparison of the electrode charge–discharge curves of the iMOF, 2,6-Naph(COOLi)$_2$, with those of other possible positive and negative intercalation electrodes with the effective potential ranges of Al and Cu current collectors. d) Discharge capacities versus cycle number of a 2,6-Naph(COOLi)$_2$/$LiNi_{0.5}Mn_{1.5}O_4$ cell. Inset: charge–discharge curves of the same cell. The cell was cycled at a rate corresponding to full charging in 5 h. e) Comparison of specific energy versus specific power plots of the stackable cell composed of a negative electrode operating at more than 0.5 V (versus Li/Li^+). f) Illustration of the prepared two-stacked 2,6-Naph(COOLi)$_2$/$LiNi_{0.5}Mn_{1.5}O_4$ bipolar cell. g) Charge–discharge curves of single and two-stacked bipolar 2,6-Naph(COOLi)$_2$/$LiNi_{0.5}Mn_{1.5}O_4$ cells using a PVdF-HFP-based gel-polymer electrolyte. The dotted line shows the half voltage of the two-stacked bipolar cell.

posed of infinite networks of metal ions connected through functionalized organic linkers to form three-dimensional networks.[10] Conventional MOFs are porous materials for gas adsorption/desorption, separation, and catalysis such as for H_2, CO, CO_2, and CH_4.[11] However, the MOFs proposed in this study show only intercalation and no gas adsorption because of their nonporous nature[12] and are thus referred to as iMOFs in the electrochemical field. We define an iMOF as having the following characteristics: 1) a layered structure consisting of organic and inorganic units, 2) intercalated Li in the inorganic layer as a result of a redox reaction of the organic layer, and 3) maintenance of the framework during Li intercalation. After exploring several π-conjugated dicarboxylate materials,[13] we selected 2,6-naphthalene dicarboxylate dilithium (2,6-Naph(COOLi)$_2$) as the negative electrode material and investigated its performance in single and bipolar cells. Furthermore, we studied in detail the mechanism for the change in the crystal structure during Li intercalation and found that the volume change of this material is extremely small.

First, a 4 V single cell was fabricated with 2,6-Naph(COOLi)$_2$ (negative) and high potential operating $LiNi_{0.5}Mn_{1.5}O_4$ spinel[14] (positive) electrodes (see Figure 1c) in a laminate-type cell. The resulting charge–discharge profile (Figure 1d, inset) demonstrates a cell voltage of 3.9 V and reproducible reversible capacity, which remained at 96% of the first-cycle capacity after 100 cycles (Figure 1d). The resulting discharge-rate performance (see Figure S1 in the Supporting Information) reveals that, by using the Al current collector for both electrodes (Figure 1e), the 2,6-Naph(COOLi)$_2$/$LiNi_{0.5}Mn_{1.5}O_4$ cells exhibit significantly higher specific energy of about 300 Wh kg^{-1} compared with the reported 3 V Li-ion battery with $Li_4Ti_5O_{12}$/$LiNi_{0.5}Mn_{1.5}O_4$ cells of about 200 Wh kg^{-1} [15] because of the higher cell voltage than that of the other cells (see Table S1 in the Supporting Information). Furthermore, the cells show

a comparably high specific power of 100 Wh kg^{-1} at about 5 kW kg^{-1} as the current electric double layer capacitors[16] or advanced capacitors, such as nano $Li_4Ti_5O_{12}$/activated carbon cells,[17] Si radical/graphite cells,[15] or nano-TiO_2-B/activated carbon cells,[18] which are candidates for high power storage applications. In addition, as shown in Figure 1 c, the operating potential of the negative electrode is expected to suppress the deposition of metallic Li (0 V), which causes internal short circuits between the positive and negative electrodes and improves the safety of the proposed bipolar battery. Moreover, by using a gel-polymer electrolyte, we fabricated two-stacked bipolar 2,6-Naph(COOLi)$_2$/$LiNi_{0.5}Mn_{1.5}O_4$ cells (Figure 1 f). We have succeeded in the construction of an 8 V bipolar cell by connecting only two cells in series in one pack (Figure 1 g).

The X-ray powder diffraction (XRD) pattern and the corresponding Rietveld refinement (Figure 2 a) confirm that 2,6-Naph(COOLi)$_2$ forms crystalline layered structures in the *a*-axis direction. The crystalline layered structures have repeating organic and inorganic units comprised of π-stacked naphthalene moieties and tetrahedral LiO_4 units (inset in Figure 2 a). The naphthalene units interact with each other through π-stacking interactions in the *b*-axis direction. The Li atoms form slightly distorted tetrahedral LiO_4 structures. The tetrahedral structures are connected by an extensive network of one edge-sharing and two corner-sharing tetrahedral LiO_4 units, which are framed by four O atoms of different naphthalene dicarboxylate units.[12a] This molecular self-assembly remains almost insoluble in common organic electrolytes. Transmission electron microscopy (TEM) images show that the material exhibits a needle-shaped crystalline structure of about 10 μm in length (Figure 2 b,c). The orientation of the needle-shaped crystal was calculated from the selected-area electron diffraction (SAED) pattern (Figure 2 d). The orientation of the crystals revealed that the longitudinal direction of the crystals was parallel to the *c*-axis, thus indicating that the 2,6-Naph(COOLi)$_2$ crystals grow in the direction of the π stacking of the naphthalene unit (Figure 2 e). High-resolution transmission electron microscopy (HRTEM) images confirm that the crystalline lattice has a neatly layered structure comprised of organic and inorganic units parallel to the direction of crystal growth (Figure 2 f).

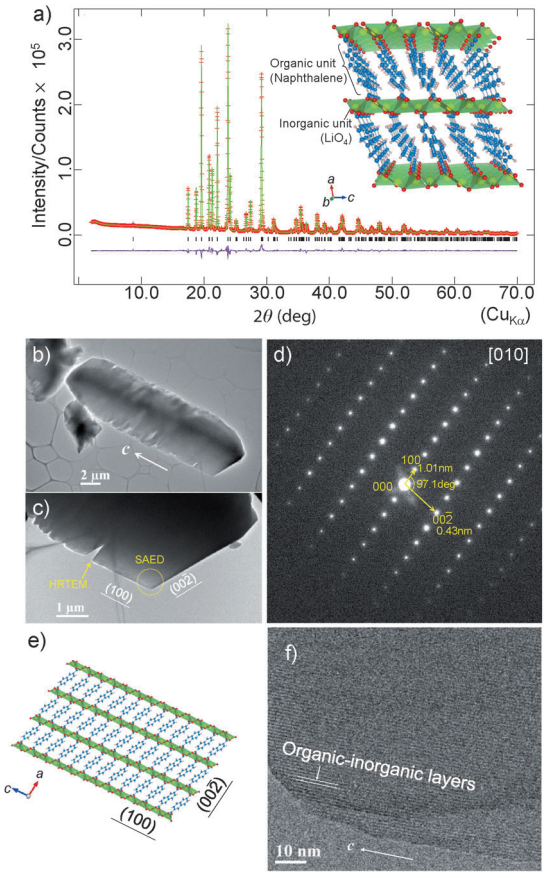

Figure 2. a) Rietveld refinement for pristine 2,6-Naph(COOLi)$_2$; the experimental powder XRD pattern (red + marks), calculated powder XRD pattern (green solid line), difference profile (pink solid line), and peak positions (tick marks). Inset: structure of the pristine sample taken from its XRD pattern (Li = yellow, O = red, C = blue, and H = white). b,c) TEM images of typical particles and d) the corresponding SAED pattern. e) Orientation of the crystalline structure of the observed particles shown in Figure 3 b,c, derived from the results of the TEM images and SAED patterns. f) HRTEM image.

The detailed crystal structure during Li intercalation was estimated from the XRD pattern and the corresponding Rietveld refinement obtained on a discharged sample. A sample for the diffraction experiment was prepared by packing the powder removed from the discharged electrode

The electrochemical performance of this sample was examined in coin-type cells using Li metal as a counter electrode. The potential–composition profile of the electrode exhibited a flat plateau near 0.8 V, with a small polarization of 70 mV (Figure 3 a). The discharge capacities for the first and second cycles were 360 and 220 mAh g^{-1}, respectively. As shown in the inset in Figure 3 a, the reversible capacity derives approximately 2 Li^+ ions per molecule, which corresponds to the theoretical capacity of this sample and is highly sustained after the second cycle (inset in Figure 3 a). 2,6-Naph(COOLi)$_2$ is superior in rate capability compared with a previously reported similar material, terephthalic acid dilithium,[6a] under the same electrochemical conditions (see Figure S2 in the Supporting Information). A potential difference and irreversible capacity can be observed in the charge–discharge curves during the first and second cycles. This phenomenon will be discussed after the structural analysis of the Li intercalation state (see Figure S6 in the Supporting Information).

To understand the detailed Li-storage mechanism further, ex situ XRD analyses of the 2,6-Naph(COOLi)$_2$ electrodes were conducted during the first discharge and charge cycles (Figure 3 b). The results show that the Li-storage phase appears during the first discharge and disappears following the charge, thereby indicating a fully reversible redox process. In addition, the crystal structure of the 2,6-Naph(COOLi)$_2$ in the composite electrode maintains unaltered before and after Li intercalation (see Figure S3 in the Supporting Information). The flat plateau of the potential–composition profile in Figure 3 a and the evolution of the XRD patterns suggests that a two-phase reaction, $C_{10}H_6(COOLi)_2 \leftrightarrow C_{10}H_6(COOLi_2)_2$, occurs.

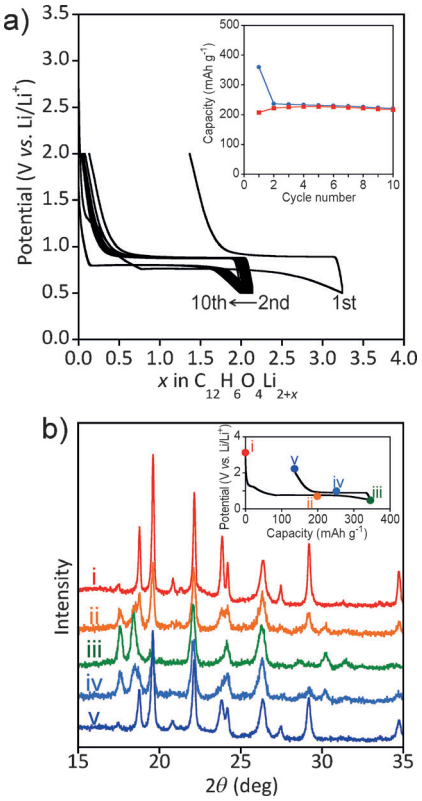

Figure 3. a) Potential–composition profile for a Li/2,6-Naph(COOLi)$_2$ cell. Inset: corresponding discharge (circles) and charge (squares) capacities versus cycle number for the same cell. b) XRD patterns for the Li/2,6-Naph(COOLi)$_2$ cell at various stages of the intercalation/deintercalation reaction.

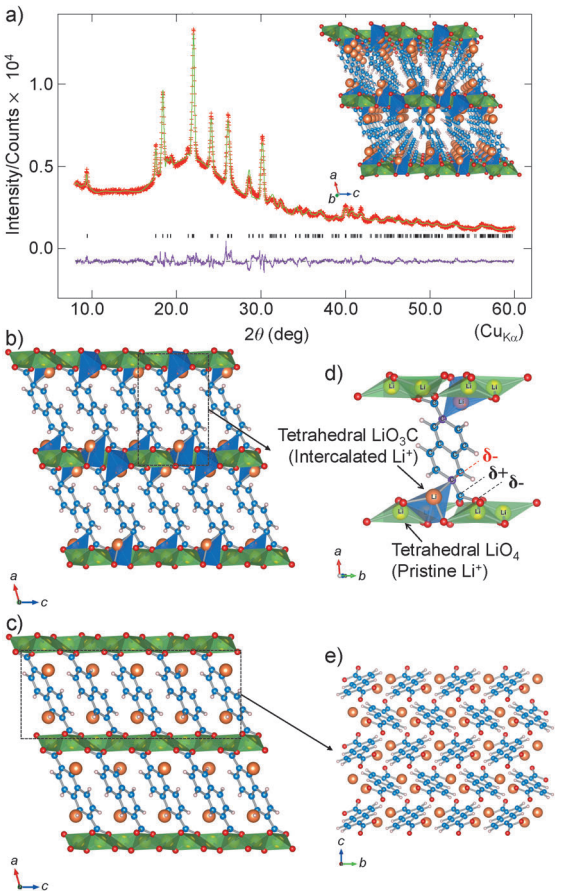

Figure 4. Structural characterization of 2,6-Naph(COOLi)$_2$ at the Li intercalated state. a) Rietveld refinement for the lithium-intercalated sample; the experimental powder XRD pattern (red + marks), calculated powder XRD pattern (green solid line), difference profile (pink solid line), and peak positions (tick marks). Inset: structure of the lithium-intercalated sample taken from its XRD pattern (intercalated Li = orange, Li = yellow, O = red, C = blue, and H = white). b,c) The structure after Li intercalation in model 1 (b) and model 2 (c) viewed along the *b*-axis direction. d,e) The coordination geometry near the intercalated Li$^+$ ions in model 1 (d) and the structure of Li-doped π-stacking naphthalene rings in model 2 (e).

into a capillary tube and was analyzed by ex situ XRD in transmission mode. The results of the Rietveld refinement indicate that the layered framework of this material was maintained during Li intercalation. As shown in Figure 4a, the results of the Rietveld refinement using first-principles calculations (see Table S2 and Figure S4a in the Supporting Information for a detailed structural optimization) indicate that there are two models for the Li intercalation state (Figure 4b,c). Model 1 (Figure 4b) shows that the intercalated Li$^+$ ions form a distorted tetrahedral LiO_3C structure and are stabilized in their respective layers. The coordination structure near the intercalated Li$^+$ ion (Figure 4d) shows the naphthalene C atom of a covalently bonded carboxylate group to have a negative charge ($C^{\delta-}$) as a result of the inductive effect of the carboxylate group, which contributes to the Li$^+$-$C^{\delta-}$ interaction. The tetrahedral LiO_3C network may be primarily responsible for the Li transport pathways (see Figure S5 in the Supporting Information). Model 2 (Figure 4c) shows that the intercalated Li$^+$ is located in the π-stacked naphthalene layer (Figure 4e). Electrochemically doping Li into the π-stacking naphthalene layer would thereby lead to electronic conduction through formation of an electron donor/acceptor complex.[19]

We found that models 1 and 2 correspond to a supplementary structure that contributes to the Li transport involved in 0.2 Li$^+$ per one molecule and a main structure that contributes to reversible capacity as well as the electron transport involved in 2 Li$^+$ per molecule, respectively (see Figure S4 in the Supporting Information). The remaining Li (0.2 Li$^+$ per one molecule) remains in the crystal structure after the initial cycle, and this is responsible for the reduction in the IV resistance of these electrodes (see Figure S6 in the Supporting Information). Rietveld refinement showed the actual density of the obtained material in the Li intercalation state to be 1.721 g cm^{-3} (see Table S3 in the Supporting Information). In terms of the energy density that takes into account the voltage and the density, 2,6-Naph(COOLi)$_2$ can be expected to have higher values of both per unit weight and volume than $Li_4Ti_5O_{12}$ (see Table S4 in the Supporting Information).

Interestingly, the Rietveld refinement results obtained from the actual experimental data of the charged and discharged samples reveal that the unit cell volume expands slightly after Li intercalation (+0.33%; see Table S3 in the

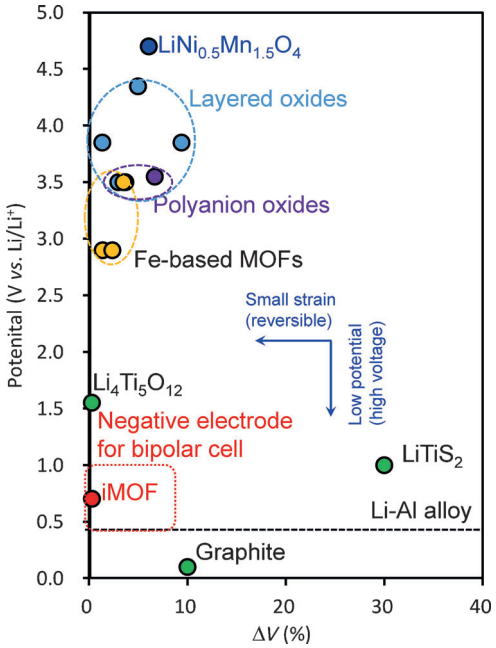

Figure 5. Comparison of the change in the volume during redox reactions and the operating potentials of a variety of intercalated electrode materials.

Supporting Information). This value is one order of magnitude lower than that of the previously reported Fe-based MOF electrodes such as $Li_xK_{0.14}Mn_{1.43}[Fe^{III}(CN)_6]$[20] or $Fe^{III}(OH)_{0.8}F_{0.2}[O_2C\text{-}C_6H_4\text{-}CO_2]$ (Figure 5).[21] Moreover, this change in volume is much lower than that of the Li-intercalated materials such as graphite carbon materials,[3] $LiNiO_2$,[22] $LiCo_{1/3}Ni_{1/3}Mn_{1/3}O_2$,[23] Li_2MnO_3-$LiCo_{1/3}Ni_{1/3}Mn_{1/3}O_2$,[24] $Li_2Ru_{1-y}Sn_yO_3$,[25] $LiNi_{0.5}Mn_{1.5}O_4$ spinel,[13c] $LiFePO_4$, or A_2FePO_4F (A = Na, Li);[26] it is comparable to that observed for $Li_4Ti_5O_{12}$, (ca. 0.3 % expansion of the unit cell;[27] the volume changes of the respective materials are shown in Table S5 in the Supporting Information). Thus, the molecular self-assembly of this material with a very small volume strain and efficient electron and Li^+ transport during Li intercalation leads to the observed electrochemical reversibility and small polarization.

With respect to the molecular design strategy for the iMOF, the naphthalene group is preferable to a benzene group for generating the Li intercalation state because the formation of the stable structures similar to model 1 and model 2 in terephthalic acid dilithium is difficult due to electrostatic repulsion. This has been confirmed from the polarization results (see Figure S2 in the Supporting Information) and the localization of electron density near the naphthalene ring that is attributed to intercalated Li (see Figure S7). The theoretical specific capacity of the active-electrode materials is reduced if the aromatic rings are extended, such as with anthracene and naphthacene. Therefore, the naphthalene ring is ideal as the organic framework in terns of both the electrostatic stability and specific capacity. Similar arguments could be made even if Li^+ was replaced by other cationic species such as Na^+, K^+, and quaternary ammonium cations.

In summary, we have demonstrated that an iMOF, 2,6-Naph$(COOLi)_2$, electrode material has a desirable operating potential of 0.5–1.0 V, which is a difficult potential with the other electrode materials used as negative electrodes for high-voltage bipolar Li-ion batteries, and shows a reversible Li intercalation mechanism. Moreover, the iMOF electrode material also maintains its framework structure during Li intercalation and is accompanied by a remarkably small volume strain, which allows both electron and Li^+ transport by molecular self-assembly, and thus provides the observed favorable cycle stability. Our results indicate that the practical application of the iMOFs will aid in the design of high energy density batteries with improved safety. Thus, we believe that these findings will create new design opportunities for high-performing batteries. iMOFs will play an important role as negative electrodes in the next generation of Li-ion batteries, especially for large-scale applications.

Received: May 9, 2014
Revised: July 29, 2014
Published online: September 2, 2014

Keywords: batteries · carboxylates · electrochemistry · intercalations · metal–organic frameworks

[1] a) M. Armand, J.-M. Tarascon, *Nature* **2008**, *451*, 652 – 657; b) B. Dunn, H. Kamath, J. M. Tarascon, *Science* **2011**, *334*, 928 – 935.
[2] M. S. Whittingham, *Chem. Rev.* **2004**, *104*, 4271 – 4301.
[3] J. Dahn, R. Fong, M. Spoon, *Phys. Rev. B* **1990**, *42*, 6424 – 6432.
[4] T. Ohzuku, A. Ueda, N. Yamamota, *J. Electrochem. Soc.* **1995**, *142*, 1431 – 1435.
[5] a) Y. Kim, J. B. Goodenough, *J. Phys. Chem. C* **2008**, *112*, 15060 – 15064; b) Y. Kim, K.-s. Park, S.-h. Song, J. Han, J. B. Goodenough, *J. Electrochem. Soc.* **2009**, *156*, A703 – 708; c) J. B. Goodenough, Y. Kim, *Chem. Mater.* **2010**, *22*, 587 – 603.
[6] a) M. Armand, S. Grugeon, H. Vezin, S. Laruelle, P. Ribiere, P. Poizot, J. M. Tarascon, *Nat. Mater.* **2009**, *8*, 120 – 125; b) W. Walker, S. Grugeon, H. Vezin, S. Laruelle, M. Armand, F. Wudl, J.-M. Tarascon, *J. Mater. Chem.* **2011**, *21*, 1615; c) L. Fedele, F. Sauvage, J. Bois, J. M. Tarascon, M. Becuwe, *J. Electrochem. Soc.* **2013**, *161*, A46 – A52.
[7] a) Y. Park, D. S. Shin, S. H. Woo, N. S. Choi, K. H. Shin, S. M. Oh, K. T. Lee, S. Y. Hong, *Adv. Mater.* **2012**, *24*, 3562 – 3567; b) A. Abouimrane, W. Weng, H. Eltayeb, Y. Cui, J. Niklas, O. Poluektov, K. Amine, *Energy Environ. Sci.* **2012**, *5*, 9632 – 9638.
[8] a) S. Wang, L. Wang, K. Zhang, Z. Zhu, Z. Tao, J. Chen, *Nano Lett.* **2013**, *13*, 4404 – 4409; b) S. Gottis, A. L. Barres, F. Dolhem, P. Poizot, *ACS Appl. Mater. Interfaces* **2014**, *6*, 10870.
[9] a) N. Ogihara, JP2011-074054, **2011**; b) N. Ogihara, WO2012/053553, **2012**.
[10] N. L. Rosi, J. Eckert, M. Eddaoudi, D. T. Vodak, J. Kim, M. O'Keeffe, O. M. Yaghi, *Science* **2003**, *300*, 1127 – 1129.
[11] a) R. Banerjee, A. Phan, B. Wang, C. Knobler, H. Furukawa, M. O'Keeffe, O. M. Yaghi, *Science* **2008**, *319*, 939 – 943; b) H. Deng, C. J. Doonan, H. Furukawa, R. B. Ferreira, J. Towne, C. B. Knobler, B. Wang, O. M. Yaghi, *Science* **2010**, *327*, 846 – 850; c) H. Furukawa, N. Ko, Y. B. Go, N. Aratani, S. B. Choi, E. Choi, A. O. Yazaydin, R. Q. Snurr, M. O'Keeffe, J. Kim, O. M. Yaghi, *Science* **2010**, *329*, 424 – 428.
[12] D. Banerjee, S. J. Kim, J. B. Parise, *Cryst. Growth Des.* **2009**, *9*, 2500 – 2503.
[13] a) J. Kaduk, *Acta Crystallogr. Sect. B* **2000**, *56*, 474 – 485; b) D. Banerjee, J. B. Parise, *Cryst. Growth Des.* **2011**, *11*, 4704 – 4720.

[14] a) Q. Zhong, A. Bonakclarpour, M. Zhang, J. R. Dahn, *J. Electrochem. Soc.* **1997**, *144*, 205 – 213; b) T. Ohzuku, S. Takeda, M. Iwanaga, *J. Power Sources* **1999**, *81 – 82*, 90 – 94; c) B. Leon, J. M. Lloris, C. P. Vicente, J. L. Tirado, *Electrochem. Solid-State Lett.* **2006**, *9*, A96 – A100.
[15] S. W. Lee, N. Yabuuchi, B. M. Gallant, S. Chen, B. S. Kim, P. T. Hammond, Y. Shao-Horn, *Nat. Nanotechnol.* **2010**, *5*, 531 – 537.
[16] H. Maruyama, H. Nakano, M. Nakamoto, A. Sekiguchi, *Angew. Chem.* **2014**, *126*, 1348 – 1352; *Angew. Chem. Int. Ed.* **2014**, *53*, 1324 – 1328.
[17] a) K. Naoi, S. Ishimoto, Y. Isobe, S. Aoyagi, *J. Power Sources* **2010**, *195*, 6250 – 6254; b) K. Naoi, S. Ishimoto, J.-i. Miyamoto, W. Naoi, *Energy Environ. Sci.* **2012**, *5*, 9363.
[18] V. Aravindan, N. Shubha, W. C. Ling, S. Madhavi, *J. Mater. Chem. A* **2013**, *1*, 6145 – 6151.
[19] a) R. S. Potember, R. C. Hoffman, H. S. Hu, J. E. Cocchiaro, C. A. Viands, T. O. Poehler, *Polym. J.* **1987**, *19*, 147 – 159; b) R. S. Potember, T. O. Poehler, R. C. Benson, *Appl. Phys. Lett.* **1982**, *41*, 548; c) R. S. Potember, T. O. Poehler, A. Rappa, D. O. Cowan, A. N. Bloch, *J. Am. Chem. Soc.* **1980**, *102*, 3659 – 3660; d) R. A. Heintz, H. Zhao, X. Ouyang, G. Grandinetti, J. Cowen, K. R. Dunbar, *Inorg. Chem.* **1999**, *38*, 144 – 156.
[20] M. Okubo, D. Asakura, Y. Mizuno, J.-D. Kim, T. Mizokawa, T. Kudo, I. Honma, *J. Phys. Chem. Lett.* **2010**, *1*, 2063 – 2071.
[21] a) G. Férey, F. Millange, M. Morcrette, C. Serre, M. L. Doublet, J. M. Greneche, J. M. Tarascon, *Angew. Chem.* **2007**, *119*, 3323 – 3327; *Angew. Chem. Int. Ed.* **2007**, *46*, 3259 – 3263; b) G. de Combarieu, M. Morcrette, F. Millange, N. Guillou, J. Cabana, C. P. Grey, I. Margiolaki, G. Ferey, J.-M. Tarascon, *Chem. Mater.* **2009**, *21*, 1602 – 1611.
[22] T. Ohzuku, A. Ueda, M. Nagayama, *J. Electrochem. Soc.* **1993**, *140*, 1862 – 1870.
[23] N. Yabuuchi, Y. Makimura, T. Ohzuku, *J. Electrochem. Soc.* **2007**, *154*, A314 – A321.
[24] N. Yabuuchi, K. Yoshii, S. T. Myung, I. Nakai, S. Komaba, *J. Am. Chem. Soc.* **2011**, *133*, 4404 – 4419.
[25] M. Sathiya, G. Rousse, K. Ramesha, C. P. Laisa, H. Vezin, M. T. Sougrati, M. L. Doublet, D. Foix, D. Gonbeau, W. Walker, A. S. Prakash, M. Ben Hassine, L. Dupont, J. M. Tarascon, *Nat. Mater.* **2013**, *12*, 827 – 835.
[26] B. L. Ellis, W. R. Makahnouk, Y. Makimura, K. Toghill, L. F. Nazar, *Nat. Mater.* **2007**, *6*, 749 – 753.
[27] a) S. Scharner, W. Weppner, P. Schmid-Beurmann, *J. Electrochem. Soc.* **1999**, *146*, 857 – 861; b) F. Ronci, P. Reale, B. Scrosati, S. Panero, V. R. Albertini, P. Perfetti, M. d. Michiel, J. M. Merino, *J. Phys. Chem. B* **2002**, *106*, 3082 – 3086.